PHYSICAL REVIEW D **92,** 075019 (2015)

Confronting Galactic center and dwarf spheroidal gamma-ray observations with cascade annihilation models

Bhaskar Dutta, Yu Gao, Tathagata Ghosh, and Louis E. Strigari

Mitchell Institute for Fundamental Physics and Astronomy, Department of Physics and Astronomy, Texas A&M University, College Station, Texas 77843-4242, USA

(Received 9 September 2015; published 15 October 2015)

Many particle dark matter models predict that the dark matter undergoes cascade annihilations, i.e. the annihilation products are 4-body final states. In the context of model-independent cascade annihilation processes, we study the compatibility of the dark matter interpretation of the Fermi-LAT Galactic center gamma-ray emission with null detections from dwarf spheroidal galaxies. For canonical values of the Milky Way density profile and the local dark matter density, we find that the dark matter interpretation to the Galactic center emission is strongly constrained. However, uncertainties in the dark matter distribution weaken the constraints and leave open dark matter interpretations over a wide range of mass scales.

DOI: 10.1103/PhysRevD.92.075019 PACS numbers: 95.35.+d, 12.60.Jv, 14.80.Ly

I. INTRODUCTION

Analyses of Fermi-LAT data have identified an emission of diffuse gamma rays distributed nearly spherically symmetric about the Galactic center, i.e. the Galactic center excess (GCE), as shown by several groups [1–3] along with Calore-Cholis-Weniger (CCW) [4]. The GCE is statistically significant, though its precise morphology and energy spectrum is still subject to systematic uncertainties that derive from the model fits. Millisecond pulsars [5], young pulsars [6], and more generally a population of point source below the Fermi-LAT threshold [7,8] have been fit to the GCE. Other astrophysical sources such as cosmic ray protons [9] and inverse Compton emission from high energy electrons [10–12] arising from burstlike events have also been discussed in the context of the GCE.

A dark matter (DM) annihilation explanation of the GCE has generated considerable excitement [13–20]. In itself, there are a couple of challenges one must confront when attempting to connect the GCE to a possible DM signal. First, the aforementioned emission from unresolved point sources and diffuse emission process are difficult to predict theoretically, which implies that the data itself is often used to understand the gamma-ray emission from these sources. Second, there is considerable freedom in DM interpretations of the excess, in that a wide range of masses and cross sections are able to fit the data.

With these points in mind, studies of other sources for a corroborating DM signal are especially important. Dwarf spheroidal galaxies (dSphs) of the Milky Way are a quintessential target for indirect DM searches [21,22], and provide an independent cross-check on a possible DM signal hinted at near the Galactic center. Indeed the lack of excess gamma-ray signal from dSphs imposes constraints on DM annihilation cross section [23], and also strongly constrains DM interpretations of the GCE for a variety of different annihilation channels with 2-body final states.

In this paper we explore DM particle models that annihilate to a pair of on-shell scalar mediators which subsequently decay into b-quarks and τ leptons, and explore their compatibility with GCE and dSph gamma-ray observations. Annihilation to 4-body final states have been considered within the context of earlier Fermi-LAT dSph observations and earlier analyses of the GCE [17,18]. In comparison to these previous papers, the goal of the paper is twofold. First we revisit the annihilation of DM into Higgs-like scalars, taking into account correlated systematic uncertainties derived by CCW. We then constrain the model parameter space using the new Fermi-LAT dSph PASS-8 results [23]. A similar study, prior to recent PASS-8 results, has been performed in the context of the next to minimal supersymmetric Standard Model [16]. In contrast, in this paper we fit the GCE in $4b$, 4τ and $2b\,2\tau$ channels in both a model-independent way and within the framework of a realistic $U(1)_{B-L}$ model incorporating all of the aforementioned decay channels.

The structure of the paper is as follows. In Sec. II we discuss our fits to the Galactic center emission and the framework for the statistical analysis. In Sec. III, we interpret the new dSph constraints in the context of our analysis. In Sec. IV we present the results of our model-independent study. In Sec. V we describe the motivation and particle content of the $U(1)_{B-L}$ model along with its possible realization in the context of GCE phenomenology. Finally we conclude in Sec. VI.

II. FITTING THE GCE WITH CASCADE ANNIHILATION THROUGH A SCALAR

The direct production of hard photons from DM annihilation is typically loop suppressed [24], so that photons produced are from decays of Standard Model (SM)

particles. Here we consider the DM particle, χ, annihilating to a pair of beyond Standard Model (BSM) scalar, ϕ, which in turn decays to various SM quarks and leptons. The continuous spectrum of gamma rays arises from light mesons, produced via hadronization and/or decay of SM fermions.

The gamma-ray differential flux from DM annihilation over a solid angle $\Delta\Omega$ is given by

$$\frac{d\Phi^{\gamma}}{dE_{\gamma}} = \frac{1}{8\pi}\frac{\langle\sigma v\rangle}{m_{\chi}^2}\sum_f \frac{dN_f^{\gamma}}{dE_{\gamma}} \times \frac{1}{\Delta\Omega}\int_{\Delta\Omega}\int_{\text{l.o.s}} \rho^2(r(s,\psi))ds d\Omega, \tag{1}$$

where the sum is extended over all annihilation channels into fermionic final states f. The first term depends on particle physics properties—$\langle\sigma v\rangle$ is the thermally averaged total cross section, m_{χ} is the DM mass, and $\frac{dN_f^{\gamma}}{dE_{\gamma}}$ is the prompt photon spectrum per annihilation into final state f. The second term, known as the astrophysical J-factor, is obtained from the line of sight integration over DM halo profile, $\rho(r(s,\psi))$, where $r(s,\psi) = \sqrt{r_{\odot}^2 + s^2 - 2r_{\odot}s\cos\psi}$, with $r_{\odot} = 8.5$ kpc and ψ being the angle from the galactic center. To provide the most straightforward comparison to previous results we utilize the generalized Navarro-Frenk-White (gNFW) profile for the DM distribution [25],

$$\rho(r) = \rho_0 \frac{(r/r_s)^{-\gamma}}{(1 + r/r_s)^{3-\gamma}}. \tag{2}$$

The scale radius r_s, is chosen to be 20 kpc, and the scale density ρ_0 is determined by fixing the local DM density at the Solar radius, $\rho_{\odot} = 0.4$ GeV/cm^3 [26]. For a DM interpretation of the GCE, the best fit is $\gamma = 1.2$ [3,4] over a region of interest (ROI) $2° \leq |b| \leq 20°$ and $|l| \leq 20°$. For these assumptions the averaged J-factor over the ROI, $\bar{J}$, is found to be 2.06×10^{23} GeV^2 cm^{-5} sr^{-1}.

To fit to the GCE, we use the results of CCW, who go into detail exploring multiple Galactic diffuse emission (GDE) models. The aforementioned analysis has been implemented by generating the prompt photon spectra using PYTHIA8.201 [27] and we verified that our results agree with PPPC4DMID [28] for $b\bar{b}$ and $\tau^+\tau^-$ final states. Next we have performed a global fit using a χ^2 statistic defined by

$$\chi^2 = \sum_{ij}\left(\frac{d\Phi_i^{\gamma}}{dE_{\gamma}} - \frac{dF_i}{dE_{\gamma}}\right)(\Sigma^{-1})_{ij}\left(\frac{d\Phi_j^{\gamma}}{dE_{\gamma}} - \frac{dF_j}{dE_{\gamma}}\right), \tag{3}$$

where $\frac{d\Phi_i^{\gamma}}{dE_{\gamma}}$ and $\frac{dF_i}{dE_{\gamma}}$ are the predicted and observed flux in the ith energy bin and Σ_{ij} is the covariance matrix containing statistical and correlated systematic errors. CCW have estimated the uncertainties of the GCE by studying 60 GDE models and also studied the correlation in the spectrum along the Galactic disk. CCW extract the residual signal and a set of systematic uncertainties, which dominates over the energy range of our interest and has a high degree of correlation across energy bins. The effects of these systematic uncertainties are included in our analysis by means of the publicly available covariance matrix, Σ_{ij} [29].

III. EXTRACTING CONSTRAINTS FROM DWARF SPHEROIDAL GALAXIES

From a combined sample of 15 dSphs, Fermi-LAT has presented the upper bounds on $\langle\sigma v\rangle$ in standard SM annihilation channels $[l^+l^-(l = e,\mu,\tau), u\bar{u}, b\bar{b}, W^+W^-]$ based on six years of data [23]. These results have improved the cross section constraints derived from previous combined samples [30–33]. Our goal is to use these bounds to estimate the sensitivity to 4-fermion final states.

To deduce constraints on 4-body final states from the published Fermi-LAT constraints on 2-body final states we utilize the following procedure. For each of the 2-body and 4-body final states that we consider we calculate the photon spectrum, $\frac{dN^{\gamma}}{dE_{\gamma}}$, and for each spectrum identify the peak energy of $E_{\gamma}^2\frac{dN^{\gamma}}{dE_{\gamma}}$, which we define as $(E_{\gamma})_{\text{max}}$. Our motivation for this definition of $(E_{\gamma})_{\text{max}}$ comes from the fact that different channels with the same $(E_{\gamma})_{\text{max}}$ have roughly the same spectral shape. For all 2-body and 4-body channels, in Fig. 1 we show $(E_{\gamma})_{\text{max}}$ as a function of the DM mass.

As an example in Fig. 2 we show the shape of both $\frac{dN^{\gamma}}{dE_{\gamma}}$ and $E_{\gamma}^2\frac{dN^{\gamma}}{dE_{\gamma}}$ for the 4τ final state with $m_{\chi} = 19$ GeV, for the $\tau^+\tau^-$ final state with $m_{\chi} = 9$ GeV, and for the $b\bar{b}$ final state with $m_{\chi} = 59$ GeV. All of these final states have the same $(E_{\gamma})_{\text{max}}$. These figures show that at asymptotically low and

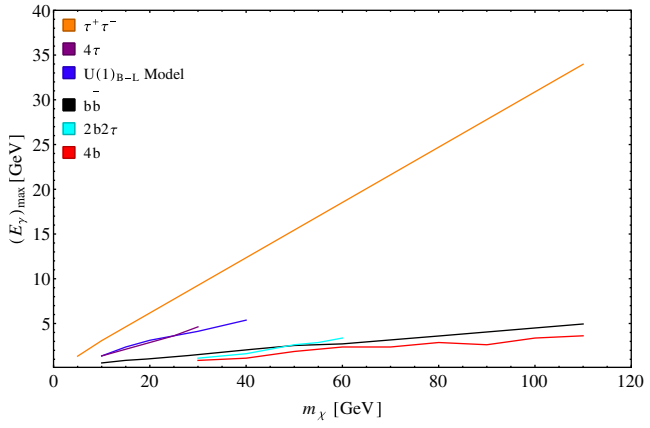

FIG. 1 (color online). The peak of $E_{\gamma}^2\frac{dN^{\gamma}}{dE_{\gamma}}$, which we define as $(E_{\gamma})_{\text{max}}$, as a function of DM mass, m_{χ}, for all 2-body and 4-body channels. The $U(1)_{B-L}$ model is described in Sec. V.

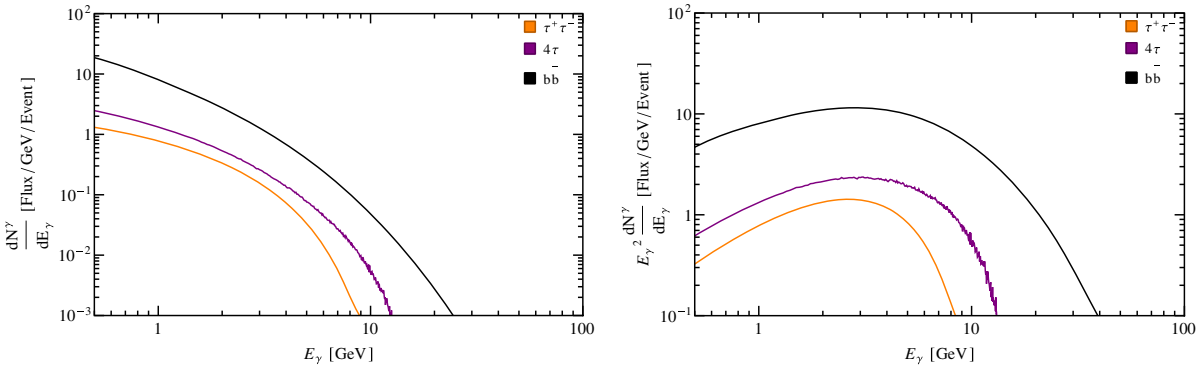

FIG. 2 (color online). The photon energy spectrum, $\frac{dN^\gamma}{dE_\gamma}$, and the spectrum weighted by the energy squared, $E_\gamma^2 \frac{dN^\gamma}{dE_\gamma}$, for 4τ (purple), $\tau^+\tau^-$ (orange) and $b\bar{b}$ (black) final states that have the same $(E_\gamma)_{\rm max}$. For 4τ channels the DM mass is $m_\chi = 19$ GeV, for the $\tau^+\tau^-$ channel it is $m_\chi = 9$ GeV, and for the $b\bar{b}$ channel it is $m_\chi = 59$ GeV.

high photon energies, the shapes of both $\frac{dN^\gamma}{dE_\gamma}$ and $E_\gamma^2 \frac{dN^\gamma}{dE_\gamma}$ for the spectra with similar $(E_\gamma)_{\rm max}$ are similar.

More generally, we derive an upper bound on $\langle\sigma v\rangle$ at a given mass $m_\chi^{\text{4-body}}$ for a 4-body final state by matching its $(E_\gamma)_{\rm max}$ with the corresponding $(E_\gamma)_{\rm max}$ of a SM 2-body final state, at a mass $m_\chi^{\text{2-body}}$ and then scaling the $\langle\sigma v\rangle$ of the 2-body final state by the ratio of the total flux in our 4-body final state to the total flux from the 2-body SM final state,

$$\langle\sigma v\rangle_{\text{4-body}} = \langle\sigma v\rangle_{\text{2-body}} \times \left(\frac{m_\chi^{\text{4-body}}}{m_\chi^{\text{2-body}}}\right)^2 \times \int_{0.5\ \text{GeV}}^{m_\chi^{\text{2-body}}} \frac{d\Phi^\gamma_{\text{2-body}}}{dE_\gamma} dE_\gamma \times \left(\int_{0.5\ \text{GeV}}^{m_\chi^{\text{4-body}}} \frac{d\Phi^\gamma_{\text{4-body}}}{dE_\gamma} dE_\gamma\right)^{-1}. \quad (4)$$

The lower photon energy limit of 0.5 GeV is motivated by the lower energy cutoff in the Fermi-LAT dSphs study [23].

The simple approach we have outlined above is used to extract plausible bounds on 4-body states without having to run through a full maximum likelihood analysis. One question that we must address is how our 4-body final state upper bounds on $\langle\sigma v\rangle$ depend on the particular choice of the 2-body final state that we use for the scaling in Eq. (4). To answer this question we have tested all 2-body scaling channels, and we generally find that the bounds obtained scaling to the $\tau^+\tau^-$ and $b\bar{b}$ 2-body final states agree within 20% of each other. In the next section our bounds are discussed in detail.

IV. RESULTS

We consider the scenario in which DM particles annihilate to produce a pair of scalars, ϕ, which then decay into a pair of quarks and leptons. For the decay of ϕ, we first explore three model independent scenarios,

$$\chi\chi \to \phi\phi, \qquad (\phi \to b\bar{b}) \quad (5)$$

$$\chi\chi \to \phi\phi, \qquad (\phi \to \tau^+\tau^-) \quad (6)$$

$$\chi\chi \to \phi_1\phi_2, \qquad (\phi_1 \to b\bar{b}, \phi_2 \to \tau^+\tau^-). \quad (7)$$

For simplicity ϕ_1 and ϕ_2 are assumed to be degenerate in mass in the case of Eq. (7). As a working example of these scenarios in Sec. V we discuss a $U(1)_{B-L}$ model, in which ϕ decays to $b\bar{b}$ and $\tau^+\tau^-$ channels with different branching ratios (BR), depending on the ϕ mass. To compare these 4-body final states to more standard 2-body final state models, we have fit the GCE in canonical $b\bar{b}$ and $\tau^+\tau^-$ annihilation channels, and for 2-body channels we find good agreement with previous results [13,15,16]. Moreover we compare our results for $4b$ and 4τ final states to previous studies [16], and find good agreement in regions where the parameter spaces coincide.

In Fig. 3 we show the annihilation cross section and the DM mass for different channels that fit the GCE at 95% C.L. As mentioned in the previous section the upper bounds on the annihilation cross section of 4-body final states are derived by scaling from upper bounds of both $b\bar{b}$ and $\tau^+\tau^-$ final states provided by Fermi-LAT. We find the bounds calculated from scaling to $b\bar{b}$ data are stronger than the same bounds computed from scaling to $\tau^+\tau^-$. In both cases, we see that there are still regions of parameter space allowed by the dSph constraints.

The $\langle\sigma v\rangle$ values for the best-fit point for each channel are tabulated in Table I, along with the corresponding $\Delta\chi^2$ values representing a measure of the goodness of fit. The upper bound on $\langle\sigma v\rangle$ for these points from the dSph constraint is also shown in Table I, and the spectra for the best-fit points are shown in Fig. 4. We note that the prompt photon spectra in Fig. 4 do not appear to be a good fit to the CCW data because only diagonal elements of the covariance matrix, Σ_{ij}, are depicted. The covariance matrix contains off-diagonal elements which are comparable to

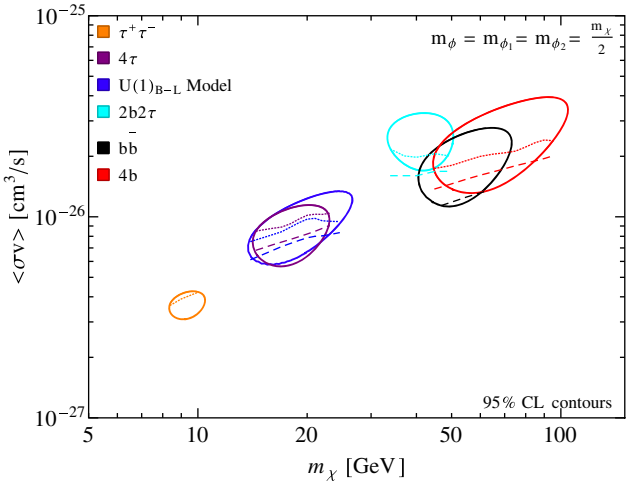

FIG. 3 (color online). Thermally averaged annihilation cross sections (95% C.L. contours) versus DM mass that fit the GCE. The dashed (dotted) lines are dSph constraints derived by scaling from $b\bar{b}$ ($\tau^+\tau^-$) limits provided by Fermi-LAT. Regions below dashed (dotted) lines are still allowed, and $m_\phi = m_{\phi_1} = m_{\phi_2}$ is set to $m_\chi/2$. The contour for the $U(1)_{B-L}$ model, described in Sec. V, are shown in dark blue.

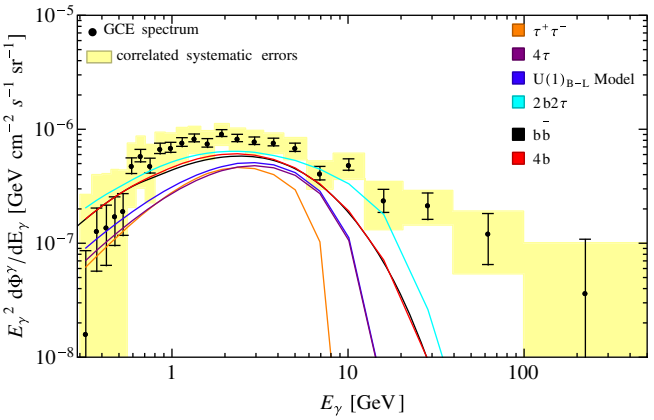

FIG. 4 (color online). The photon spectra for the best-fit values of $(m_\chi, \langle\sigma v\rangle)$ for all channels shown in Table I. The GCE data together with statistical and systematic errors [4] has been used and $m_\phi = m_{\phi_1} = m_{\phi_2}$ has been set to $m_\chi/2$ for these fits.

the diagonal elements because of the strong correlation of the systematic errors across energy bins. When the full covariance matrix is taken into account in the $\Delta\chi^2$ computation, the result is a more reasonable measure of goodness of fit, as shown in Table I.

For the analysis in Fig. 3 and Table I, the mass of the scalar mediators $m_\phi = m_{\phi_1} = m_{\phi_2}$ are set to $m_\chi/2$. To investigate the impact of the mass of these scalar mediators, we have fit to the GCE and evaluated the corresponding $\Delta\chi^2$, with different m_ϕ values for our best-fit points in all 4-body channels. We show these results in Table II for the $4b$ and 4τ channels. From Table II it is evident that the best fit to the GCE is obtained for $m_\phi \sim m_\chi/2$. We verified that the conclusions are similar for the $2b\,2\tau$ channel as well.

Our results agree with previous studies in that light mediators are favored by the GCE [17,18]. However, we favor a lower boost factor, which is defined as $\gamma_{\rm boost} \simeq 4m_\chi^2/(4m_\phi m_\chi)$. For instance, Ref. [17] shows that the GCE prefers $m_\phi \sim 2m_b$ (with $\gamma_{\rm boost} \sim 7$) or $m_\phi \sim m_\chi$ using the data of Ref. [3]. For comparison our analysis shows $\gamma_{\rm boost} \sim 2$ is preferred by the GCE.

We find that by including the correlated systematics of CCW, the GCE is better fit by a relatively broad spectrum for $m_\phi \sim m_\chi/2$. Different masses of ϕ broaden out the spectrum, as is illustrated in Fig. 5 for the best-fit points ($m_\chi = 65$ GeV and 19 GeV) in $4b$ and 4τ final states respectively. Evidently the output of the CCW data is best fit by the broadest spectrum arising for $m_\phi = m_\chi/2$. For comparison the narrower spectra of $m_\phi = m_\chi/4$ and $m_\phi \approx m_\chi$ do not provide as good of a fit to the data. For a more detailed comparison of these two data sets, together with Fermi-LAT's analysis of the GCE [34], we refer to Refs. [15,19,35].

Let us now consider the results from Table I and Fig. 3 in more detail. From Table I we notice that the $\phi\phi \to 4b$ final state offers the best fit to the CCW GCE data, with a best fit mass and cross section of $m_\chi = 65$ GeV and

TABLE I. Best-fit results of spectral fits to the Fermi Galactic center excess in different channels, together with 95% C.L. limits and the upper bound on $\langle\sigma v\rangle$, coming from dSphs, for the corresponding point. The upper bounds on the annihilation cross section of 4-body final states are derived by scaling from upper bounds of both $b\bar{b}$ and $\tau^+\tau^-$ final states provided by Fermi-LAT and shown under columns named $b\bar{b}$ and $\tau^+\tau^-$ respectively. $m_\phi = m_{\phi_1} = m_{\phi_2} = m_\chi/2$ is assumed for these points. The results for the $U(1)_{B-L}$ model are also shown in the Table.

	Best fit			dSphs allowed	
				$b\bar{b}$	$\tau^+\tau^-$
Channel	m_χ (GeV)	$\langle\sigma v\rangle$ (10^{-26} cm^3 s^{-1})	$\Delta\chi^2_{\rm min}$	$\langle\sigma v\rangle_{\rm max}$ (10^{-26} cm^3 s^{-1})	
$\tau^+\tau^-$	9	0.36	33.4	⋯	0.39
4τ	19	0.90	28.2	0.78	0.95
$U(1)_{B-L}$	19	0.97	27.5	0.75	0.91
$2b\,2\tau$	41	2.43	26.7	1.64	2.01
$b\bar{b}$	50	1.80	25.2	1.18	⋯
$4b$	65	2.45	23.1	1.64	1.99

TABLE II. The dependence of goodness of fit on the mass of the scalar mediator, ϕ, for the best-fit point ($m_\chi = 65$ GeV and 19 GeV) in $4b$ and 4τ channels respectively.

	Best fit			
	$4b$		4τ	
m_ϕ (GeV)	$\langle\sigma v\rangle$ (10^{-26} cm^3 s^{-1})	$\Delta\chi^2_{\rm min}$	$\langle\sigma v\rangle$ (10^{-26} cm^3 s^{-1})	$\Delta\chi^2_{\rm min}$
$m_\chi/4$	2.14	27.7	0.86	29.0
$m_\chi/2$	2.45	23.1	0.90	28.2
$3m_\chi/4$	2.58	26.3	0.86	28.9
$\approx m_\chi$	2.39	33.7	0.78	32

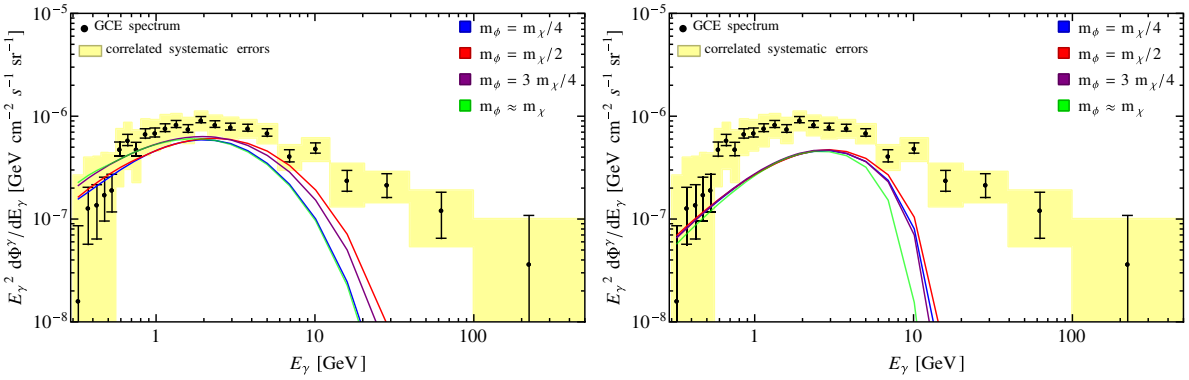

FIG. 5 (color online). The photon spectra in $4b$ (left) and 4τ (right) final states for different values of mediator mass m_ϕ. m_χ has been set to its best-fit value of 65 GeV (19 GeV) for $4b$ (4τ) channel and best fit $\langle\sigma v\rangle$ for each value of m_ϕ has been used in this plot.

$\langle\sigma v\rangle = 2.45 \times 10^{-26}$ cm^3/s, respectively. The $b\bar{b}$ final state also provides a good fit to the data for $m_\chi = 50$ GeV and $\langle\sigma v\rangle = 1.80 \times 10^{-26}$ cm^3/s. The GCE can be explained by a wide range of DM mass for $\langle\sigma v\rangle \sim 1.27 - 4 \times 10^{-26}$ cm^3/s ($4b$ channel) and $\langle\sigma v\rangle \sim 1.08 - 2.76 \times 10^{-26}$ cm^3/s ($2b$ channel) respectively at 95% C.L. The $4b$ channel allows the widest range of DM mass, 45–103 GeV, while $b\bar{b}$ fits for 43–73 GeV. The dSph constraint also allows a larger area in the $m_\chi - \langle\sigma v\rangle$ plane for the $4b$ final state as compared to the $b\bar{b}$ final state. However for both channels the best-fit $\langle\sigma v\rangle$ value from the GCE is disallowed by the dSph constraint. The $\phi_1\phi_2 \to 2b2\tau$ final state fits the data as well for $m_\chi \sim 37$–50 GeV with $\langle\sigma v\rangle \sim 1.53 - 3.3 \times 10^{-26}$ cm^3/s at 95% C.L., with a best fit obtained for $m_\chi = 41$ GeV. The dSph constraint derived from $b\bar{b}$ rules out the entire $m_\chi - \langle\sigma v\rangle$ plane in the parameter space, while the constraint from $\tau^+\tau^-$ allows a small fraction of it.

In a similar manner, the $\phi\phi \to 4\tau$ final state allows for a wider range of DM mass (15–23 GeV), as opposed to a very narrow window (8.4–10.4 GeV) for the $\tau^+\tau^-$ final state. There is a slightly larger range of $\langle\sigma v\rangle$ values preferred by the 4τ channel ($0.56 - 1.19 \times 10^{-26}$ cm^3/s) relative to the 2τ channel ($0.31 - 0.43 \times 10^{-26}$ cm^3/s). However, while almost the entire parameter space is allowed for the $\tau^+\tau^-$ final state for our choice of γ and ρ_0 (previously observed by Ref. [35]), an appreciable area of the 4τ final state is ruled out by the dSph constraint.

To this point we have neglected two effects which may have an impact on our results. The first is the effect of inverse Compton scattering (ICS). ICS modifies the observed photon spectrum, typically by ∼10% for final states involving τ's. It is less significant when considering final states with b-quarks. The impact of ICS on the GCE has been discussed in detail [13].

In addition the results we have presented assume gNFW profile, which is shown to provide the best fit for the GCE [3,4]. There is of course a significant uncertainty in the average J-factor, $\bar{J}$, within the ROI that we consider, because of the uncertain DM distribution near the Galactic center. The impact of this uncertainty has been previously quantified, so that $\bar{J}$ anywhere from 0.19 to 3 times the canonical value that we use is allowed [15]. The impact of this variation in J-factor on our fit to the GCE and

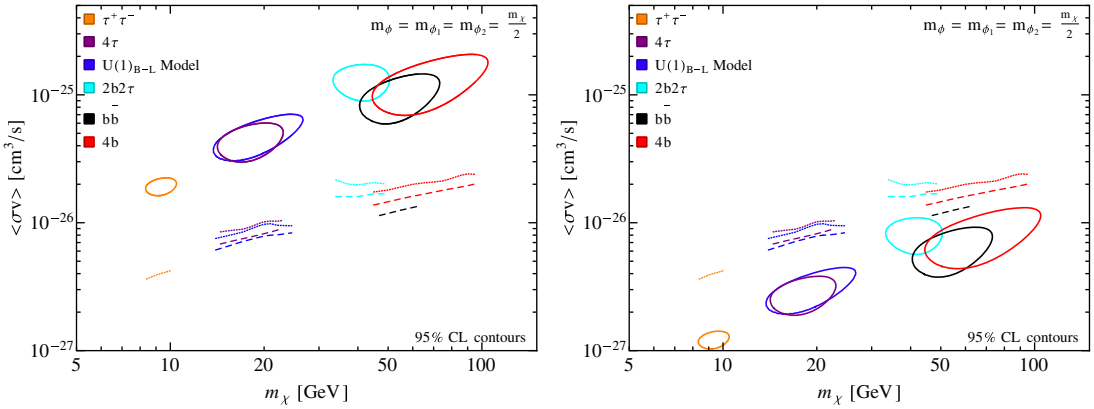

FIG. 6 (color online). Thermally averaged annihilation cross sections (95% C.L. contours) versus DM mass that fit the GCE, along with corresponding dSphs constraints if extreme values of J-factor are used. In the left panel $\bar{J} = 4 \times 10^{22}$ GeV^2 cm^{-5} sr^{-1} ($\rho_\odot = 0.2$ GeV/cm^3, $\gamma = 1.1$), and in the right panel 6.07×10^{23} GeV^2 cm^{-5} sr^{-1} ($\rho_\odot = 0.6$ GeV/cm^3, $\gamma = 1.3$). Dashed and dotted lines representing dSph constraints have the same meaning as in Fig. 3. Here we also take $m_\phi = m_{\phi_1} = m_{\phi_2}$ is set to $m_\chi/2$.

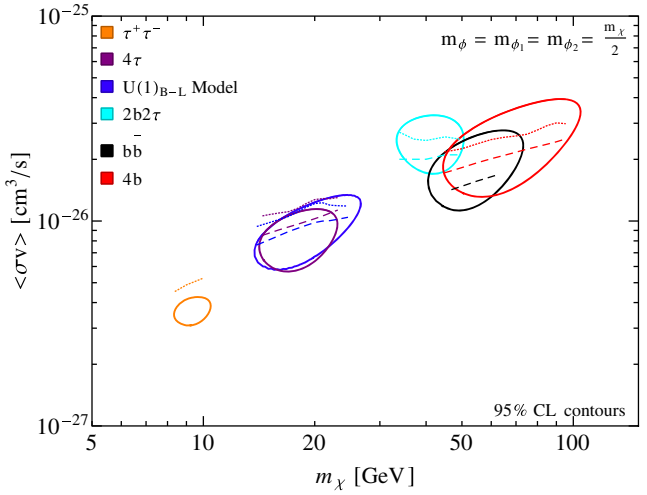

FIG. 7 (color online). The dSph constraints on the parameter space that fits GCE, if Burkert DM profile is used for dSphs. Dashed and dotted lines representing dSph constraints have the same meaning as in Fig. 3. As above we take $m_\phi = m_{\phi_1} = m_{\phi_2}$ is set to $m_\chi/2$.

the corresponding dSph constraint is shown in Fig. 6. We conclude from Fig. 6 that, with different choices for the parameters of the gNFW profile, the dSph constraint can either exclude or allow the entire parameter space that fits GCE. Also assuming a Burkert model for the dSphs relaxes this bound by ∼25% [23]. The effect of these relaxed bounds on our results are presented in Fig. 7.

V. $U(1)_{B-L}$ MODEL

Now we move on to consider an example of an extended minimal supersymmetric Standard Model (MSSM) model where the lightest right-handed sneutino is the DM candidate. This model provides a case of a cascade model to complement the model-independent approach highlighted above. The well motivated $B-L$ extension of the MSSM [36] explains the neutrino masses and mixings since it has three right-handed (RH) neutrinos. The minimal model contains a new gauge boson Z' belonging to the extended $U(1)_{B-L}$ sector. The anomaly cancellation of $U(1)_{B-L}$ requires three RH neutrinos N together with their supersymmetric partners $\tilde{N}$. The model may further contain two new Higgs fields H_1' and H_2' (the presence of two Higgsinos are again required by anomaly cancellation), with rich phenomenological implications [37–39].

The superpotential is given by $W = W_{\rm MSSM} + W_{B-L} + y_D \mathbf{N^c H_u L}$, where $\mathbf{L}$ and $\mathbf{H_u}$ are the superfields, which contain the Higgs fields and provide mass to the left-handed leptons and up-type quarks respectively. The W_{B-L} term consists of $\mathbf{H_1'}$, $\mathbf{H_2'}$ and $\mathbf{N^c}$. Charge assignments of the new Higgs fields determine the detailed form of W_{B-L}, e.g.,

Fields	Q	Q^c	L	L^c	H_1'	H_2'
Q_{B-L}	1/6	−1/6	−1/2	1/2	3/2	−3/2

The scalar potential is comprised of D-terms from the gauge symmetries, and F-terms from the superpotential. The D-term contribution of $U(1)_{B-L}$ is given by $V_D \supset \frac{1}{2} D_{B-L}^2$, where $D_{B-L} = \frac{1}{2} g_{B-L}[Q_1(|H_1'|^2 - |H_2'|^2) + \frac{1}{2}|\tilde{N}|^2 + \cdots]$. Here g_{B-L} is the $U(1)_{B-L}$ gauge coupling, and Q_1, $-Q_1$, 1/2 are the $B-L$ charges of H_1', H_2', $\tilde{N}$ respectively. The vacuum expectation value (VEV) of H_1' and H_2', denoted by v_1' and v_2' respectively, breaks $U(1)_{B-L}$ and provides a mass ($m_{Z'} = g_{B-L} Q_1 \sqrt{v_1'^2 + v_2'^2}$) for the Z'. There are three physical Higgs fields ϕ, Φ (scalars) and $\mathcal{A}$ (a pseudoscalar) in the extended Higgs sector. The scalar potential leads to the coupling between the RH sneutrinos and the new Higgs particles.

The sneutrino, $\tilde{N}$, is a natural candidate for DM in this model [37]. [The lightest neutralino in the extended sector, which is a superposition of the two Higgsinos $\tilde{H}_1'$, $\tilde{H}_2'$ and the $U(1)_{B-L}$ gaugino $\tilde{Z}'$, can also be a possible candidate [38,39].] The dominant annihilation channel of the DM particle is $\tilde{N}^*\tilde{N} \to \phi\phi$ via the contact term $|\tilde{N}|^2\phi^2$, the s-channel exchange of the ϕ, Φ, and the t, u-channel exchange of the $\tilde{N}$. Here ϕ is the lightest of the new scalars. The s-channel Z' exchange is suppressed due to the large experimental bound on the Z' mass. $\tilde{N}^*\tilde{N} \to \phi\Phi, \phi\mathcal{A}, \Phi\Phi, \mathcal{A}\mathcal{A}$ annihilation processes are also possible, but they are either kinematically not favored or/and forbidden for the parameter space under consideration. Although the sneutrinos can also annihilate to RH neutrinos, N (via t-channel neutralino exchange), but again for the parameter space that we consider the annihilation into $\phi\phi$ final states is dominant. Other fermion-antifermion final states, feasible through s-channel Z' exchange, have even smaller BRs. Moreover they are p-wave suppressed.

The 4-fermion final state appears in $\tilde{N}^*\tilde{N}$ annihilation due to the subsequent decay of ϕ into fermion-antifermion pairs via a one-loop diagram involving two Z' bosons. The decay rate is given by $\Gamma(\phi \to f\bar{f}) = \frac{C_f}{2^7\pi^5} \frac{g_{B-L}^6 Q_f^4 Q_\phi^2 m_\phi^5 m_f^2}{m_{Z'}^6} (1 - \frac{4m_f^2}{m_\phi^2})^{3/2}$, where C_f denotes color factor, Q_f and Q_ϕ are the $B-L$ charges of the final state fermion and the ϕ respectively, and m_f is the fermion mass [37,38]. Evidently the leptonic BR is larger than that for quarks due to 3 times larger $B-L$ charge of leptons compared to quarks. We should point out that m_ϕ is regulated by the VEVs of the new Higgs fields and for $\tan\beta' \approx 1$, i.e. when the VEVs are comparable, it can be very small compared to $m_{Z'}$. The dominant decay mode of ϕ is $\phi \to \tau^-\tau^+$ for $m_\phi > 2m_b$. The BR of ϕ as a function of m_ϕ is shown in Fig. 8, with $m_{Z'} = 2.1$ TeV [40] and $g_{B-L} = 0.4$. For the mass range of interest for the GCE study, $\phi \to \tau^+\tau^-$ BR is ∼80 − 90%.

Using reasonable values for the model parameters, i.e., $\tan\beta' \approx 1$, soft gaugino mass $M_{\tilde{Z}'} \geq 500$ GeV, soft masses for the Higgs fields $m_{H_{1,2}'} = 200$–600 GeV,

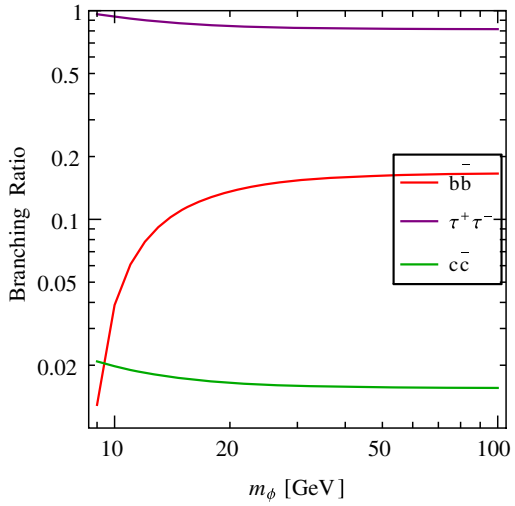

FIG. 8 (color online). Branching ratio of ϕ in different fermion-antifermion pairs as a function of mass.

$\mu' = 0.5$–2 TeV (μ' being the Higgs mixing parameter in the $B-L$ sector), and $m_{Z'} > 1.5$ TeV, we find that the thermal relic abundance can be satisfied in this model with the DM mass, $m_{\tilde{N}} \sim 10$–60 GeV which we will use for our analysis. Since we consider $\tilde{N}^*\tilde{N} \to \phi\phi$, m_ϕ is smaller than the DM mass. We use $g_{B-L} \sim 0.3$–0.4 for the relic density calculation, which is in concordance with unification of the gauge couplings [37]. The large Z' mass in this model also allows us to satisfy the direct detection [41] and collider bounds [42–44].

We are now in position to describe our results for the $U(1)_{B-L}$ model, which includes all 4-body channels discussed in Sec. IV. The DM annihilation spectra arising from the model are dictated by the $\tilde{N}^*\tilde{N} \to \phi\phi \to 4\tau$ process with 80%–90% probability. Hence one may suspect that the set of $(m_{\tilde{N}}, \langle\sigma v\rangle)$ values of the model that fit the GCE should be very similar to the 4τ case and this fact is demonstrated in Fig. 3 and Table I. Similar to the 4τ case the best fit to the GCE is obtained for $m_{\tilde{N}} = 19$ GeV. Although $\tilde{N}$ mass of 14.5–25 GeV fit the GCE excess with $\langle\sigma v\rangle \sim 0.58 - 1.42 \times 10^{-26}$ cm^3/s, only a fraction of it is allowed by dSphs.

Though we discuss the B-L model for the DM annihilation to $4b$, 4τ, $2b\,2\tau$ final states with specific BRs of $\phi \to b\bar{b}$ and $\phi \to \tau^+\tau^-$ determined by the B-L charges, the analysis that we have presented in the previous two sections can be used for other models since we show our results for generic BRs of the scalar state ϕ to $b\bar{b}$ and $\tau^+\tau^-$ final states.

VI. CONCLUSION

In this paper we performed a model-independent fit to the GCE for DM particles annihilating to $4b$, 4τ and $2b\,2\tau$ final states by means of cascade annihilation through a pair of BSM scalars ϕ (two scalars ϕ_1, ϕ_2 for $2b\,2\tau$ final state). We compared these results with standard $b\bar{b}$ and $\tau^+\tau^-$ final states. We also presented a well motivated $U(1)_{B-L}$ model, where the lightest right-handed sneutrino ($\tilde{N}$) is the DM candidate, which provides a realistic scenario incorporating all 4-body final states mentioned above. The main result of this paper is the constraint imposed on the $m_\chi - \langle\sigma v\rangle$ plane for aforementioned 4-body channels by the reprocessed Fermi-LAT PASS-8 data on dwarf spheroidal galaxies.

We found a wide range of DM masses that fit the GCE in 4-body final states with distinct range of annihilation cross sections characteristic of the final state. However a considerable area of the $m_\chi - \langle\sigma v\rangle$ plane is disallowed by the dSph constraint, strongly constraining the DM interpretation of the GCE. The scalar masses have limited impact on the analysis but $m_\phi \sim m_\chi/2$ provides the best fit to the spectra. The impact of ICS is also negligible for the final states under consideration.

The $4b$ channel provides the best fit for $m_\chi \sim 45$–103 GeV and $\langle\sigma v\rangle \sim 1.27 - 4 \times 10^{-26}$ cm^3/s at 95% C.L. with the upper half of the parameter space ruled out by dSphs. The $2b\,2\tau$ channel fits the excess for $m_\chi \sim 37$–50 GeV and $\langle\sigma v\rangle \sim 1.53 - 3.3 \times 10^{-26}$ cm^3/s. Compared to the $4b$ final state, the dSphs are found to be considerably more constraining for $2b\,2\tau$ and $b\bar{b}$ channels. On the other hand they are a less stringent constraint for the 4τ final state. Out of the 95% C.L. fit of $m_\chi \sim 15$–23 GeV and $\langle\sigma v\rangle \sim 0.56 - 1.19 \times 10^{-26}$ cm^3/s, a large area in the $m_\chi - \langle\sigma v\rangle$ plane remains available if bounds are derived by scaling from the $\tau^+\tau^-$ channel. However the $\tau^+\tau^-$ channel remains unconstrained. The $U(1)_{B-L}$ model mostly follows the 4τ channel for $m_{\tilde{N}} \sim 14.5 - 25$ GeV, which fits the GCE.

ACKNOWLEDGMENTS

We thank Tracy Slatyer for helpful discussions. This work is supported by DOE Grant No. DE-FG02-13ER42020, NSF Grant No. PHY-1522717 and support from the Mitchell Institute. Y. G. thanks the Mitchell Institute for Fundamental Physics and Astronomy for support.

[1] L. Goodenough and D. Hooper, Possible evidence for dark matter annihilation in the inner Milky Way from the Fermi gamma ray space telescope, arXiv:0910.2998; D. Hooper and L. Goodenough, Dark matter annihilation in the Galactic center as seen by the Fermi gamma ray space telescope, Phys. Lett. B **697**, 412 (2011).

[2] A. Boyarsky, D. Malyshev, and O. Ruchayskiy, A comment on the emission from the Galactic center as seen by the Fermi telescope, Phys. Lett. B **705**, 165 (2011); D. Hooper and T. Linden, On the origin of the gamma rays from the galactic center, Phys. Rev. D **84**, 123005 (2011); K. N. Abazajian and M. Kaplinghat, Detection of a gamma-ray source in the Galactic center consistent with extended emission from dark matter annihilation and concentrated astrophysical emission, Phys. Rev. D **86**, 083511 (2012); **87**, 129902(E) (2013); B. Zhou, Y. F. Liang, X. Huang, X. Li, Y. Z. Fan, L. Feng, and J. Chang, GeV excess in the Milky Way: Depending on diffuse galactic gamma ray emission template?, Phys. Rev. D **91**, 123010 (2015).

[3] T. Daylan, D. P. Finkbeiner, D. Hooper, T. Linden, S. K. N. Portillo, N. L. Rodd, and T. R. Slatyer, The characterization of the gamma-ray signal from the central Milky Way: A compelling case for annihilating dark datter, arXiv: 1402.6703.

[4] F. Calore, I. Cholis, and C. Weniger, Background model systematics for the Fermi GeV excess, J. Cosmol. Astropart. Phys. 03 (2015) 038; C. Gordon and O. Macias, Dark matter and pulsar model constraints from Galactic center Fermi-LAT gamma ray observations, Phys. Rev. D **88**, 083521 (2013); **89**, 049901(E) (2014).

[5] K. N. Abazajian, The consistency of Fermi-LAT observations of the Galactic center with a millisecond pulsar population in the central stellar cluster, J. Cosmol. Astropart. Phys. 03 (2011) 010; C. Gordon and O. Macias, Dark matter and pulsar model constraints from Galactic center Fermi-LAT gamma ray observations, Phys. Rev. D **88**, 083521 (2013); **89**, 049901(E) (2014); K. N. Abazajian, N. Canac, S. Horiuchi, and M. Kaplinghat, Astrophysical and dark matter interpretations of extended gamma-ray emission from the Galactic center, Phys. Rev. D **90**, 023526 (2014); Q. Yuan and B. Zhang, Millisecond pulsar interpretation of the Galactic center gamma-ray excess, J. High Energy Astrophys. **3–4**, 1 (2014); T. D. Brandt and B. Kocsis, Disrupted globular clusters can explain the Galactic center gamma ray excess, arXiv:1507.05616.

[6] R. M. O'Leary, M. D. Kistler, M. Kerr, and J. Dexter, Young pulsars and the Galactic center GeV gamma-ray excess, arXiv:1504.02477.

[7] R. Bartels, S. Krishnamurthy, and C. Weniger, Strong support for the millisecond pulsar origin of the Galactic center GeV excess, arXiv:1506.05104.

[8] S. K. Lee, M. Lisanti, B. R. Safdi, T. R. Slatyer, and W. Xue, Evidence for unresolved gamma-ray point sources in the inner galaxy, arXiv:1506.05124.

[9] E. Carlson and S. Profumo, Cosmic ray protons in the inner galaxy and the Galactic center gamma-ray excess, Phys. Rev. D **90**, 023015 (2014).

[10] I. Cholis, C. Evoli, F. Calore, T. Linden, C. Weniger, and D. Hooper, The Galactic center GeV Excess from a series of leptonic cosmic-ray outbursts, arXiv:1506.05119.

[11] J. Petrovic, P. D. Serpico, and G. Zaharijas, Galactic center gamma-ray "excess", from an active past of the Galactic center?, J. Cosmol. Astropart. Phys. 10 (2014) 052.

[12] D. Gaggero, M. Taoso, A. Urbano, M. Valli, and P. Ullio, Towards a realistic astrophysical interpretation of the Galactic center excess, arXiv:1507.06129.

[13] F. Calore, I. Cholis, C. McCabe, and C. Weniger, A Tale of tails: Dark matter interpretations of the Fermi GeV excess in light of background model systematics, Phys. Rev. D **91**, 063003 (2015).

[14] I. Cholis, D. Hooper, and T. Linden, Challenges in explaining the Galactic center gamma-ray excess with millisecond pulsars, J. Cosmol. Astropart. Phys. 06 (2015) 043; F. Calore, M. Di Mauro, and F. Donato, Gamma rays from Galactic pulsars, arXiv:1412.4997.

[15] P. Agrawal, B. Batell, P. J. Fox, and R. Harnik, WIMPs at the Galactic center, J. Cosmol. Astropart. Phys. 05 (2015) 011.

[16] D. G. Cerdeno, M. Peiro, and S. Robles, Fits to the Fermi-LAT GeV excess with RH sneutrino dark matter: Implications for direct and indirect dark matter searches and the LHC, Phys. Rev. D **91**, 123530 (2015).

[17] A. Berlin, P. Gratia, D. Hooper, and S. D. McDermott, Hidden sector dark matter models for the Galactic center gamma-ray excess, Phys. Rev. D **90**, 015032 (2014).

[18] P. Ko, W. I. Park, and Y. Tang, Higgs portal vector dark matter for GeV scale γ-ray excess from Galactic center, J. Cosmol. Astropart. Phys. 09 (2014) 013; C. Bohm, M. J. Dolan, and C. McCabe, A weighty interpretation of the Galactic center excess, Phys. Rev. D **90**, 023531 (2014); M. Abdullah, A. DiFranzo, A. Rajaraman, T. M. P. Tait, P. Tanedo, and A. M. Wijangco, Hidden on-shell mediators for the Galactic center γ-ray excess, Phys. Rev. D **90**, 035004 (2014); A. Martin, J. Shelton, and J. Unwin, Fitting the Galactic center gamma-ray excess with cascade annihilations, Phys. Rev. D **90**, 103513 (2014).

[19] J. M. Cline, G. Dupuis, Z. Liu, and W. Xue, Multimediator models for the Galactic center gamma ray excess, Phys. Rev. D **91**, 115010 (2015).

[20] L. A. Anchordoqui and B. J. Vlcek, W-WIMP annihilation as a source of the Fermi bubbles, Phys. Rev. D **88**, 043513 (2013); W. C. Huang, A. Urbano, and W. Xue, Fermi bubbles under dark matter scrutiny part II: Particle physics analysis, J. Cosmol. Astropart. Phys. 04 (2014) 020; A. Hektor and L. Marzola, Coy dark matter and the anomalous magnetic moment, Phys. Rev. D **90**, 053007 (2014); A. Alves, S. Profumo, F. S. Queiroz, and W. Shepherd, Effective field theory approach to the Galactic center gamma-ray excess, Phys. Rev. D **90**, 115003 (2014); A. Berlin, D. Hooper, and S. D. McDermott, Simplified dark matter models for the Galactic center gamma-ray excess, Phys. Rev. D **89**, 115022 (2014); P. Agrawal, B. Batell, D. Hooper, and T. Lin, Flavored dark matter and the Galactic center gamma-ray excess, Phys. Rev. D **90**, 063512 (2014); E. Izaguirre, G. Krnjaic, and B. Shuve, The Galactic center excess from the bottom up, Phys. Rev. D **90**, 055002 (2014); D. G. Cerdeo, M. Peir, and S. Robles, Low-mass right-handed sneutrino dark matter: SuperCDMS and LUX constraints and the Galactic center gamma-ray excess, J. Cosmol. Astropart. Phys. 08 (2014) 005; S. Ipek, D. McKeen, and A. E. Nelson, A renormalizable model for

the Galactic center gamma ray excess from dark matter annihilation, Phys. Rev. D **90**, 055021 (2014); D. K. Ghosh, S. Mondal, and I. Saha, Confronting the Galactic center gamma ray excess with a light scalar dark matter, J. Cosmol. Astropart. Phys. 02 (2015) 035; L. Wang and X. F. Han, A simplified 2HDM with a scalar dark matter and the galactic center gamma-ray excess, Phys. Lett. B **739**, 416 (2014); B. D. Fields, S. L. Shapiro, and J. Shelton, Galactic Center Gamma-Ray Excess from Dark Matter Annihilation: Is there a Black Hole Spike?, Phys. Rev. Lett. **113**, 151302 (2014); C. Arina, E. Del Nobile, and P. Panci, Dark Matter with Pseudoscalar-Mediated Interactions Explains the DAMA Signal and the Galactic Center Excess, Phys. Rev. Lett. **114**, 011301 (2015); C. Cheung, M. Papucci, D. Sanford, N. R. Shah, and K. M. Zurek, NMSSM interpretation of the Galactic center excess, Phys. Rev. D **90**, 075011 (2014); J. Huang, T. Liu, L. T. Wang, and F. Yu, Supersymmetric subelectroweak scale dark matter, the Galactic center gamma-ray excess, and exotic decays of the 125 GeV Higgs boson, Phys. Rev. D **90**, 115006 (2014); P. Ko and Y. Tang, Galactic center γ-ray excess in hidden sector DM models with dark gauge symmetries: Local Z_3 symmetry as an example, J. Cosmol. Astropart. Phys. 01 (2015) 023; S. Baek, P. Ko, and W. I. Park, Local Z_2 scalar dark matter model confronting galactic GeV-scale γ-ray and muon $(g-2)$, Phys. Lett. B **747**, 255 (2015); N. Okada and O. Seto, Galactic center gamma-ray excess from two-Higgs-doublet-portal dark matter, Phys. Rev. D **90**, 083523 (2014); K. Ghorbani, Fermionic dark matter with pseudo-scalar Yukawa interaction, J. Cosmol. Astropart. Phys. 01 (2015) 015; N. F. Bell, S. Horiuchi, and I. M. Shoemaker, Annihilating asymmetric dark matter, Phys. Rev. D **91**, 023505 (2015); A. D. Banik and D. Majumdar, Low energy gamma ray excess confronting a singlet scalar extended inert doublet dark matter model, Phys. Lett. B **743**, 420 (2015); D. Borah and A. Dasgupta, Galactic center gamma ray excess in a radiative neutrino mass model, Phys. Lett. B **741**, 103 (2015); J. H. Yu, Vector fermion-portal dark matter: Direct detection and Galactic center gamma-ray excess, Phys. Rev. D **90**, 095010 (2014); J. Guo, J. Li, T. Li, and A. G. Williams, NMSSM explanations of the Galactic gamma ray excess and promising LHC searches, Phys. Rev. D **91**, 095003 (2015); J. Cao, L. Shang, P. Wu, J. M. Yang, and Y. Zhang, Supersymmetry explanation of the Fermi Galactic center excess and its test at LHC run II, Phys. Rev. D **91**, 055005 (2015); M. Heikinheimo and C. Spethmann, Galactic center GeV Photons from dark technicolor, J. High Energy Phys. 12 (2014) 084; K. Cheung, W. C. Huang, and Y. L. S. Tsai, Non-abelian dark matter solutions for galactic gamma-ray excess and Perseus 3.5 keV X-ray line, J. Cosmol. Astropart. Phys. 05 (2015) 053; A. Berlin, A. DiFranzo, and D. Hooper, A 3.55 keV line from exciting dark matter without a hidden sector, Phys. Rev. D **91**, 075018 (2015); C. H. Chen and T. Nomura, $SU(2)_X$ vector DM and Galactic center gamma-ray excess, Phys. Lett. B **746**, 351 (2015); K. P. Modak and D. Majumdar, Confronting galactic and extragalactic γ-ray observed by Fermi-LAT with annihilating dark matter in inert Higgs doublet model, Astrophys. J. Suppl. Ser. **219**, 37 (2015); A. Achterberg, S. Caron, L. Hendriks, R. Ruiz de Austri, and C. Weniger, A description of the Galactic center excess in the minimal supersymmetric standard model, J. Cosmol. Astropart. Phys. 08 (2015) 006; A. Berlin, S. Gori, T. Lin, and L. T. Wang, Pseudoscalar portal dark matter, Phys. Rev. D **92**, 015005 (2015); T. Gherghetta, B. von Harling, A. D. Medina, M. A. Schmidt, and T. Trott, SUSY implications from WIMP annihilation into scalars at the Galactic center, Phys. Rev. D **91**, 105004 (2015); J. Guo, Z. Kang, P. Ko, and Y. Orikasa, Accidental dark matter: Case in the scale invariant local $B-L$ model, Phys. Rev. D **91**, 115017 (2015); A. Rajaraman, J. Smolinsky, and P. Tanedo, On-shell mediators and top-charm dark matter models for the Fermi-LAT Galactic center excess, arXiv:1503.05919; E. C. F. S. Fortes, V. Pleitez, and F. W. Stecker, Secluded WIMPs, QED with massive photons, and the galactic center gamma-ray excess, arXiv:1503.08220; P. Ko and Y. Tang, Dark Higgs channel for FERMI GeV γ-ray excess, arXiv:1504.03908; J. Kim, J. C. Park, and S. C. Park, Galactic center GeV gamma-ray excess from dark matter with gauged lepton numbers, arXiv:1505.04620; C. Balzs, T. Li, C. Savage, and M. White, Interpreting the Fermi-LAT gamma ray excess in the simplified framework, arXiv:1505.06758; J. Cao, L. Shang, P. Wu, J. M. Yang, and Y. Zhang, Interpreting the Galactic center gamma-ray excess in the NMSSM, arXiv:1506.06471; A. Butter, T. Plehn, M. Rauch, D. Zerwas, S. Henrot-Versill, and R. Lafaye, Invisible Higgs decays to Hooperons in the NMSSM, arXiv:1507.02288; D. Kim and J. C. Park, Energy peak: Back to the Galactic center GeV gamma-ray excess, arXiv:1507.07922; N. Fonseca, L. Necib, and J. Thaler, Dark matter, shared asymmetries, and galactic gamma ray signals, arXiv:1507.08295; M. R. Buckley and D. Feld, Dark matter in leptophilic Higgs models after the LHC Run-I, arXiv:1508.00908; K. P. Modak, D. Majumdar, and S. Rakshit, A possible explanation of low energy γ-ray excess from galactic center and Fermi bubble by a dark matter model with two real scalars, J. Cosmol. Astropart. Phys. 03 (2015) 011; A. D. Banik, D. Majumdar, and A. Biswas, Possible explanation of indirect gamma ray signatures from hidden sector $\mathbf{SU}(2)_\mathbf{H}$ fermionic dark matter, arXiv:1506.05665; A. Biswas, Explaining low energy gamma-ray excess from the Galactic center using a two component dark matter model, arXiv:1412.1663; A. Biswas, D. Majumdar, and P. Roy, Nonthermal two component dark matter model for Fermi-LAT ray excess and 3.55 keV X-ray line, J. High Energy Phys. 04 (2015) 065; E. Hardy, R. Lasenby, and J. Unwin, Annihilation signals from asymmetric dark matter, J. High Energy Phys. 07 (2014) 049.

[21] L. E. Strigari, Galactic searches for dark matter, Phys. Rep. **531**, 1 (2013).

[22] J. Conrad, J. Cohen-Tanugi, and L. E. Strigari, WIMP searches with gamma rays in the Fermi era: Challenges, methods and results, arXiv:1503.06348.

[23] M. Ackermann *et al.* (Fermi-LAT Collaboration), Searching for dark matter annihilation from Milky Way dwarf spheroidal galaxies with six years of Fermi-LAT data, Astrophys. J. **809**, L4 (2015).

[24] L. Bergstrom, Dark matter evidence, particle physics candidates and detection methods, Ann. Phys. (Berlin) **524**, 479 (2012).

[25] J. F. Navarro, C. S. Frenk, and S. D. M. White, The structure of cold dark matter halos, Astrophys. J. **462**, 563 (1996);
A universal density profile from hierarchical clustering, Astrophys. J. **490**, 493 (1997).
[26] J. Bovy and S. Tremaine, On the local dark matter density, Astrophys. J. **756**, 89 (2012).
[27] T. Sjöstrand, S. Ask, J. R. Christiansen, R. Corke, N. Desai, P. Ilten, S. Mrenna, S. Prestel, C. O. Rasmussen, and P. Z. Skands, An Introduction to PYTHIA 8.2, Comput. Phys. Commun. **191**, 159 (2015).
[28] M. Cirelli, G. Corcella, A. Hektor, G. Hütsi, M. Kadastik, P. Panci, M. Raidal, F. Sala, and A. Strumia, PPPC 4 DM ID: A poor particle physicist cookbook for dark matter indirect detection, J. Cosmol. Astropart. Phys. 03 (2011) 051; 10 (2012) E01(E); P. Ciafaloni, D. Comelli, A. Riotto, F. Sala, A. Strumia, and A. Urbano, Weak corrections are relevant for dark matter indirect detection, J. Cosmol. Astropart. Phys. 03 (2011) 019.
[29] F. Calore, I. Cholis, and C. Weniger, https://staff.fnwi.uva.nl/c.weniger/pages/material/.
[30] M. Ackermann *et al.* (Fermi-LAT Collaboration), Dark matter constraints from observations of 25 Milky Way satellite galaxies with the Fermi large area telescope, Phys. Rev. D **89**, 042001 (2014).
[31] A. Geringer-Sameth and S. M. Koushiappas, Exclusion of Canonical WIMPs by the Joint Analysis of Milky Way Dwarfs with Fermi, Phys. Rev. Lett. **107**, 241303 (2011).
[32] M. Ackermann *et al.* (Fermi-LAT Collaboration), Constraining Dark Matter Models from a Combined Analysis of Milky Way Satellites with the Fermi Large Area Telescope, Phys. Rev. Lett. **107**, 241302 (2011).
[33] A. Geringer-Sameth, S. M. Koushiappas, and M. G. Walker, A comprehensive search for dark matter annihilation in dwarf galaxies, Phys. Rev. D **91**, 083535 (2015).
[34] S. Murgia, Observation of the high energy gamma-ray emission towards the Galactic center, http://fermi.gsfc.nasa.gov/science/mtgs/symposia/2014/program/08_Murgia.pdf.
[35] M. Wood, New Fermi-LAT results on the search for dark matter annihilation in dwarf spheroidal galaxies, https://indico.cern.ch/event/344116/material/slides/0.pdf.
[36] R. N. Mohapatra and R. E. Marshak, Local $B-L$ Symmetry of Electroweak Interactions, Majorana Neutrinos, and Neutron Oscillations, Phys. Rev. Lett. **44**, 1316 (1980); **44**, 1644(E) (1980).
[37] R. Allahverdi, B. Dutta, K. Richardson-McDaniel, and Y. Santoso, Sneutrino dark matter and the observed anomalies in cosmic rays, Phys. Lett. B **677**, 172 (2009).
[38] R. Allahverdi, B. Dutta, K. Richardson-McDaniel, and Y. Santoso, A supersymmetric B^- L dark matter model and the observed anomalies in the cosmic rays, Phys. Rev. D **79**, 075005 (2009).
[39] S. Khalil and H. Okada, Dark matter in $B-L$ extended MSSM models, Phys. Rev. D **79**, 083510 (2009).
[40] A. Alves, A. Berlin, S. Profumo, and F. S. Queiroz, Dark matter complementarity and the Z' portal, arXiv:1501.03490.
[41] D. S. Akerib *et al.* (LUX Collaboration), First Results from the LUX Dark Matter Experiment at the Sanford Underground Research Facility, Phys. Rev. Lett. **112**, 091303 (2014).
[42] T. Aaltonen *et al.*, Search for New Physics in High Mass Electron-Positron Events in $p\bar{p}$ Collisions at $\sqrt{s} = 1.96$-TeV, Phys. Rev. Lett. **99**, 171802 (2007).
[43] M. S. Carena, A. Daleo, B. A. Dobrescu, and T. M. P. Tait, Z' gauge bosons at the Tevatron, Phys. Rev. D **70**, 093009 (2004).
[44] Y. A. Coutinho, E. C. F. S. Fortes, and J. C. Montero, Z'_{B-L} phenomenology at LHC, Phys. Rev. D **84**, 055004 (2011); **84**, 059901 (2011).